Electronic Supplementary Material (ESI) for Energy & Environmental Science.
This journal is © The Royal Society of Chemistry 2018

Supporting Information

Enhanced Solar Cells Stability by Hygroscopic Polymer Passivation of Metal Halide Perovskite Thin Film

Min Kim[1], Silvia G. Motti[1,2], Roberto Sorrentino[1,2], Annamaria Petrozza[1]*

[1] Center for Nano Science and Technology @Polimi, Istituto Italiano di Tecnologia, via Giovanni Pascoli 70/3, 20133, Milan, Italy.

[2] Dipartimento di Fisica, Politecnico di Milano, Piazza L. da Vinci, 32, 20133 Milano, Italy.

Figure S1. Water contact angles of the polymer thin films (PEO: left, PS: right) on glass.

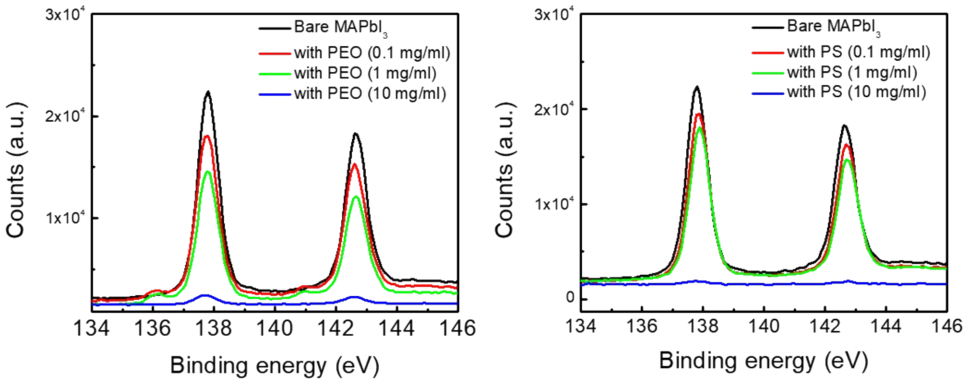

Figure S2. XPS spectra of $MAPbI_3$ covered with PEO or PS.

Table S1. Relative atomic concentrations (at%) determined by XPS of perovskite film covered by polymer films (φ = the degree of coverage)

Polymer	Concentration ($mg \cdot ml^{-1}$)	[C] (at%)	[O] (at%)	[N] (at%)	[I] (at%)	[Pb] (at%)	φ
None	0	25.39	3.92	14.08	43.47	13.14	-
PEO	0.1	32.53	11.24	12.14	33.72	10.38	0.21
	1	37.22	15.38	10.38	28.01	9	0.32
	10	73.75	24.52	0.54	0.83	0.36	0.97
PS	0.1	34.83	4.1	12.25	37.49	11.33	0.14
	1	53.58	1.68	10.1	26.15	8.49	0.35
	10	98.07	0.21	1.58	0.13	0.02	0.99

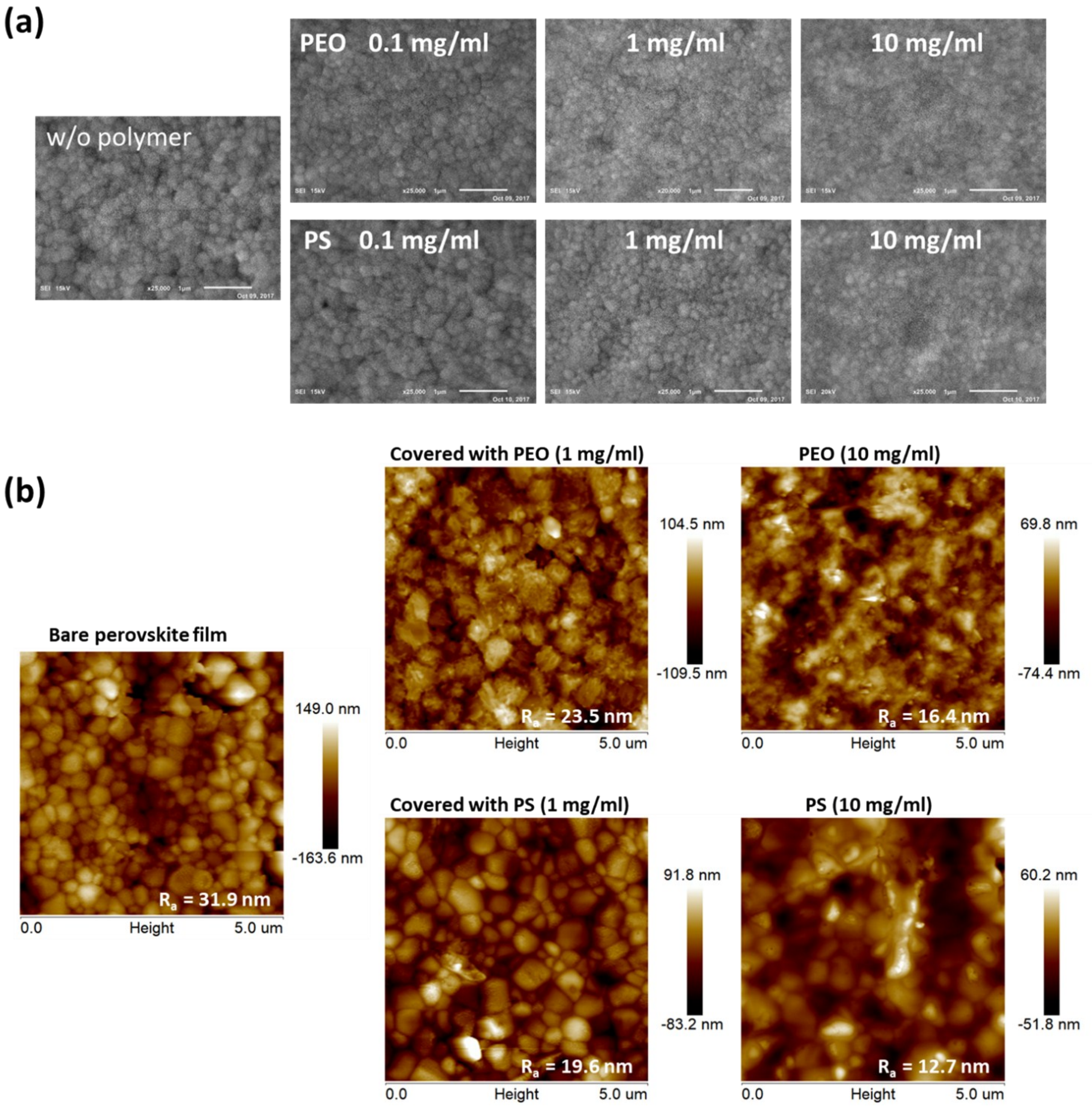

Figure S3. (a) SEM and (b) AFM images of $MAPbI_3$ coated with polymer thin films from various concentrations.

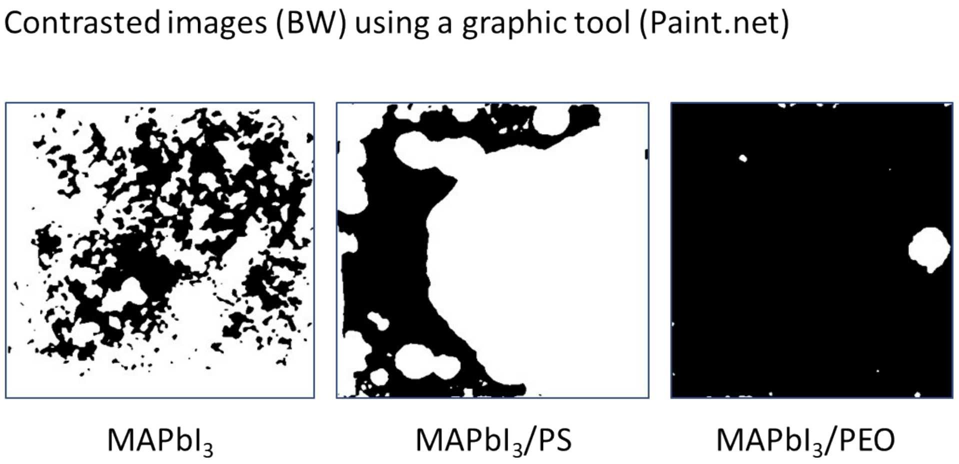

$MAPbI_3$ $MAPbI_3/PS$ $MAPbI_3/PEO$

Figure S4. Contrasted and inverted photographs of $MAPbI_3$ coated without or with PEO and PS. The films are degraded in high relative humidity of 88% for 14 days.

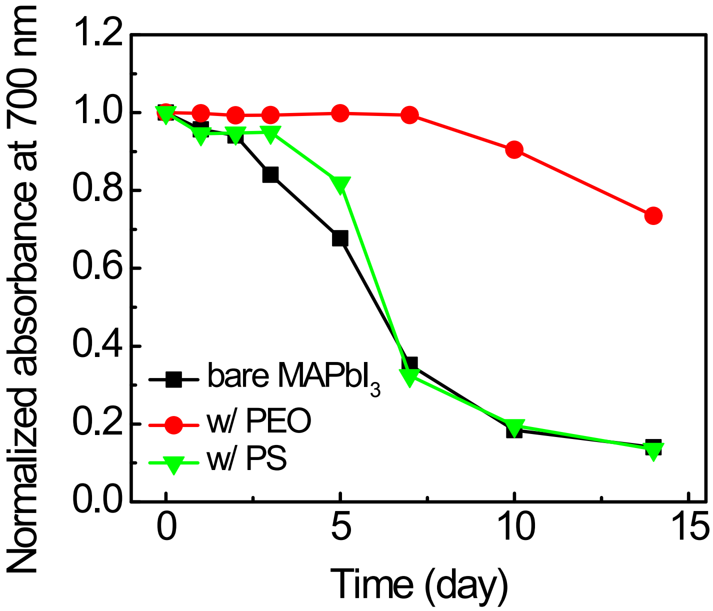

Figure S5. Normalized absorbance at 700 nm as a function of time for perovskite films exposed to relative humidity of 88%.

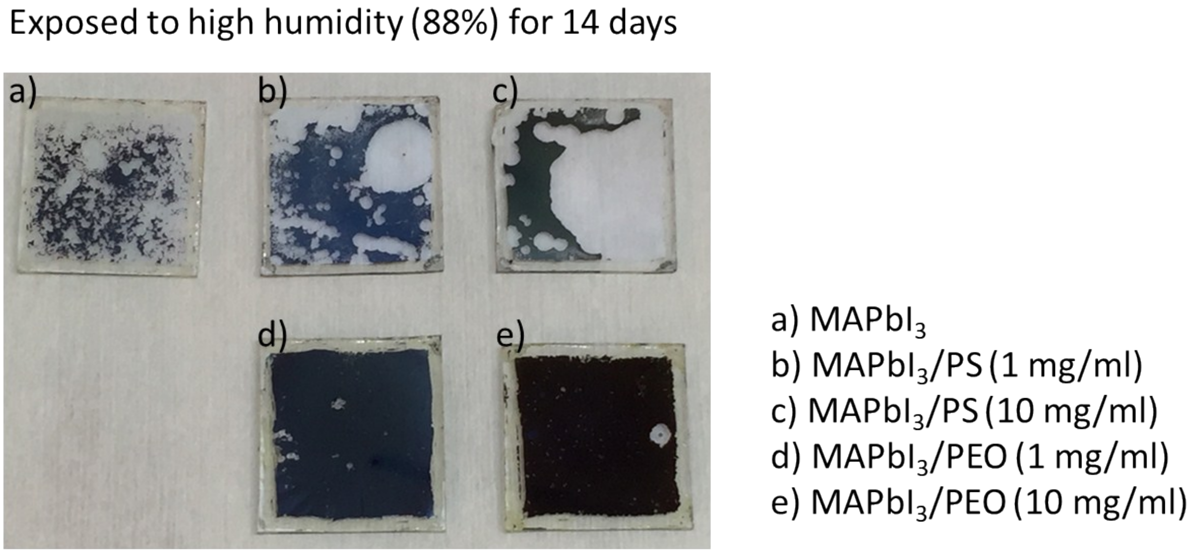

Figure S6. Photographs of MAPbI$_3$ coated with polymer thin films from various concentrations. The films are degraded after exposure to high relative humidity for 14 days.

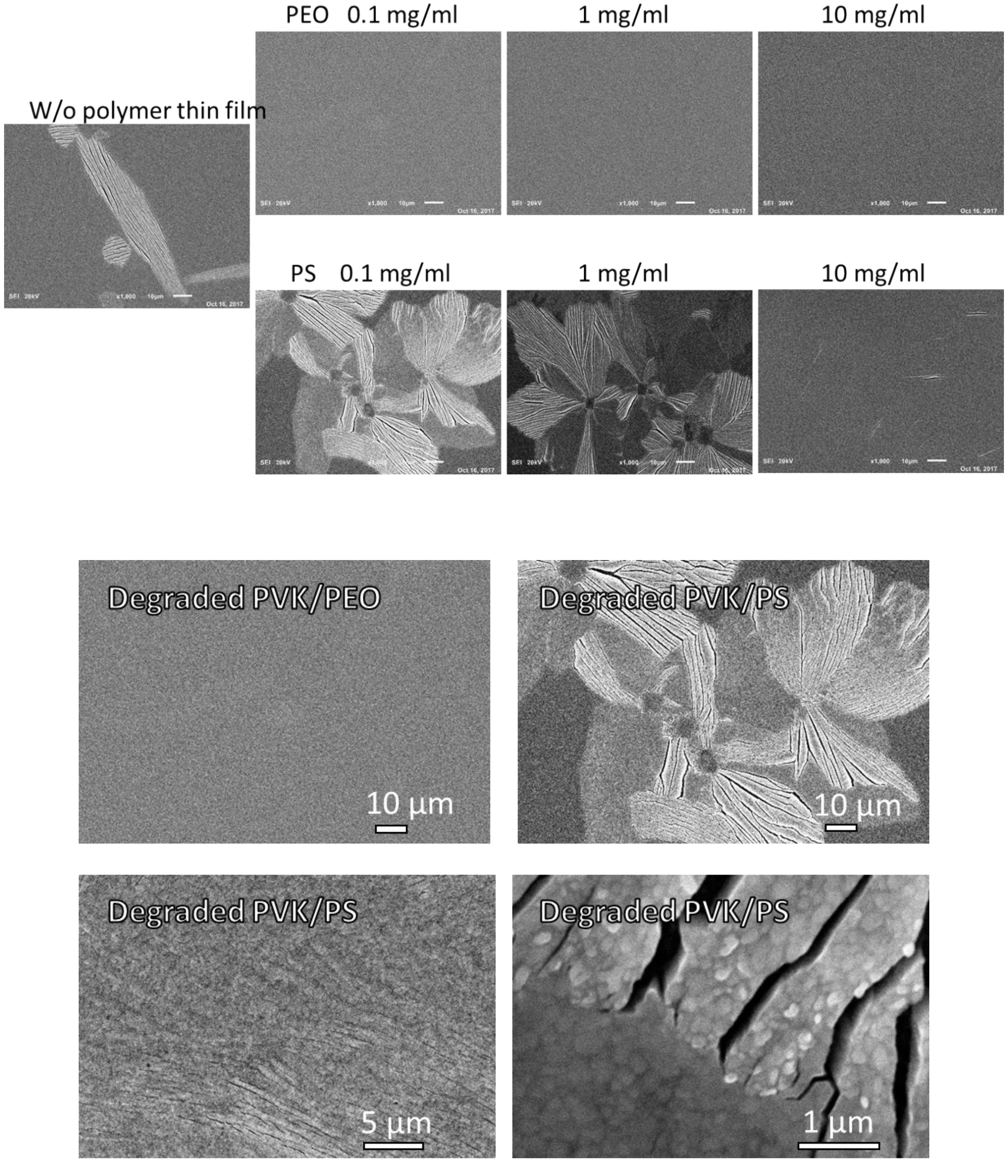

Figure S7. SEM images of the degraded $MAPbI_3$ with or without PEO and PS. The films are exposed to high relative humidity of 88% for 4 days.

Figure S6 shows top-view SEM images obtained for the degraded perovskites passivated with the polymer, PEO and PS, deposited on glass/cTiO_2/C_{60} after moisture exposure for 4 days. Even after moisture exposure, the $MAPbI_3$/PEO film still showed homogeneous and pinhole-free with a grain size of 200 ~ 400 nm. However, in the $MAPbI_3$/PS film, dramatic morphological changes were observed after moisture exposure. The hydrated perovskite formed large defect formations with a dendritic shape. The brighter region near the line-featured defects is due to less conductive and accumulates charges injected. The formation of line defects was originated from the volumetric expansion of the hydrated perovskite phases, ~28%, which makes perovskite form wrinkle-like delamination from the substrate.[A. M. A. Leguy et al., *Chem. Mater.* 2015, 27, 3397] These structural changes with the needle-like formation of hydrated perovskites were also previously observed by Yang et al., in whose study perovskite films were exposed to high humidity. [J. Yang et al., *ACS Nano* 2015, 9, 1955] With a closer look at high magnification, it was observed that the original perovskite crystal whose size is 200 to 400 nm did not change much after degradation. It explains that the hydration of perovskite layer started at the grain boundaries which is the weakest place to get deformed when the volumetric film changes. This morphological change was also identically observed in the as-prepared perovskite without polymer passivation after degradation (Fig. S6). The PS thin film on perovskite could not hinder the penetration of water molecules towards the underlying perovskite layer. Even the perovskite completely covered with PS (10 mg/ml) also developed these moisture-driven degradations.

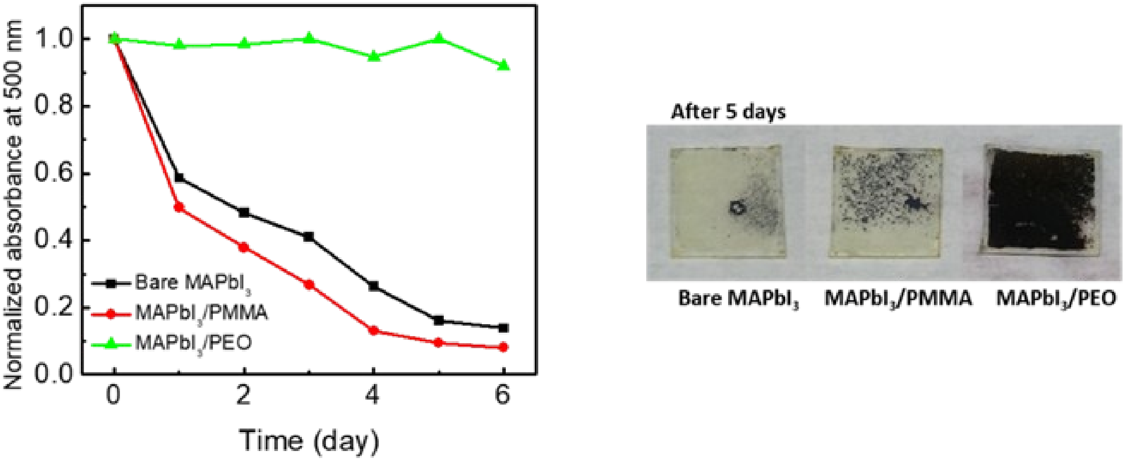

Figure S8. The time-dependent absorbance of the perovskite films with polymer passivation, PEO and PMMA.

Table S2. Fitting parameters extracted from biexponential decay function.

$$Y = A_1 \mathrm{exp}\left(-t_1 X\right) + A_2 \mathrm{exp}\left(-t_2 X\right)$$

Excitation density (uW/cm^2)	Reference		MAPbI$_3$/PEO		MAPbI$_3$/PS	
3	A_1	0.395	A_1	0.509	A_1	0.454
	t_1 (ns)	153.42	t_1 (ns)	364.85	t_1 (ns)	3.45
	A_2	0.519	A_2	0.303	A_2	0.493
	t_2 (ns)	4.48	t_2 (ns)	47.19	t_2 (ns)	74.02
10	A_1	0.574	A_1	0.610	A_1	0.622
	t_1 (ns)	165.95	t_1 (ns)	352.99	t_1 (ns)	80.94
	A_2	0.334	A_2	0.200	A_2	0.341
	t_2 (ns)	5.087	t_2 (ns)	46.35	t_2 (ns)	5.19
30	A_1	0.645	A_1	0.167	A_1	0.661
	t_1 (ns)	162.10	t_1 (ns)	58.40	t_1 (ns)	83.39
	A_2	0.259	A_2	0.658	A_2	0.262
	t_2 (ns)	6.83	t_2 (ns)	327.38	t_2 (ns)	4.21
100	A_1	0.184	A_1	0.205	A_1	0.190
	t_1 (ns)	26.76	t_1 (ns)	53.47	t_1 (ns)	6.94
	A_2	0.619	A_2	0.610	A_2	0.730
	t_2 (ns)	175.51	t_2 (ns)	257.20	t_2 (ns)	96.69

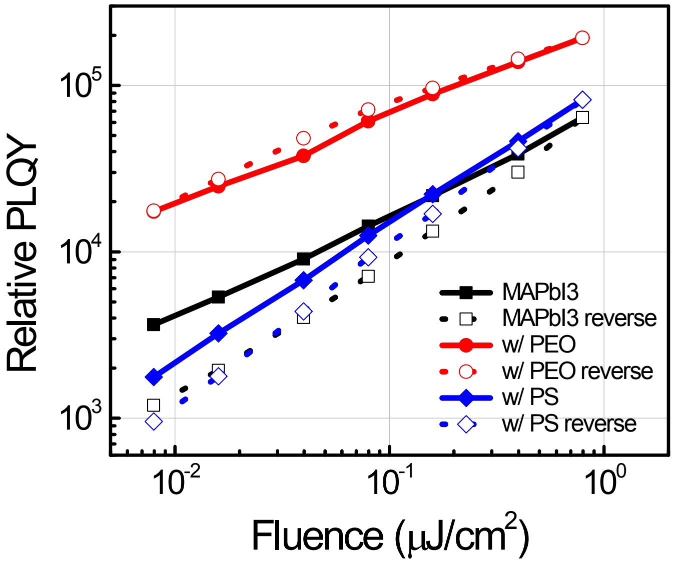

Figure S9. Relative PLQY curves of MAPbI3 thin films with and without polymer passivation.

Figure S9 shows the relative PLQY of $MAPbI_3$ thin films, which is calculated as the integrated PL intensity divided by the excitation intensity, and plotted as a function of fluence, in the range between 10^{-2} and 1 $\mu J \cdot cm^{-2}$ (continuous wave (CW) illumination, corresponding to photon densities between ~10^{20} to 10^{22} cm^{-3}). To exclude the effect of oxygen in the air, the samples were kept and measured in vacuum (pressure <10^{-5} mbar).[1] The solid lines show the PLQY collected with increasing excitation intensity from 10^{-2} to 1 $\mu J \cdot cm^{-2}$, while the dashed lines show the data collected when the excitation intensity decreases from 1 to 10^{-2} $\mu J \cdot cm^{-2}$. The reference $MAPbI_3$ shows an increasing trend of PLQYs from low to high excitation intensities. This result originates from the effect of filling trap states with higher carrier densities.[2, 3] However, the reference $MAPbI_3$ shows a steeper decreasing trend of the PLQYs when scanned from high to low excitation intensities, in which each of the PLQY values measured on the forward scan is always higher than that measured on the reverse scan. After the complete intensity sweep, the relative PLQY drops by three-fold at the fluence of 10^{-2} $\mu J \cdot cm^{-2}$. This suggests that the density of traps increases under photoexcitation.[1] The PEO-capped perovskite behaves differently from the reference. The PLQY value of the PEO-$MAPbI_3$ film increases with respect to those of the reference, and the hysteretic behavior totally disappears. These results infer that the PEO thin polymer heals defect states on the thin film surface by effective suppression of non-radiative recombination paths. By contrast, the PS-capped perovskite film is even less emissive than the reference sample at low excitation intensities and also shows strong PL hysteresis. These are all evidence that PS, once in contact with a perovskite thin film, modifies the semiconductor interface creating loss channels for photogenerated carriers.

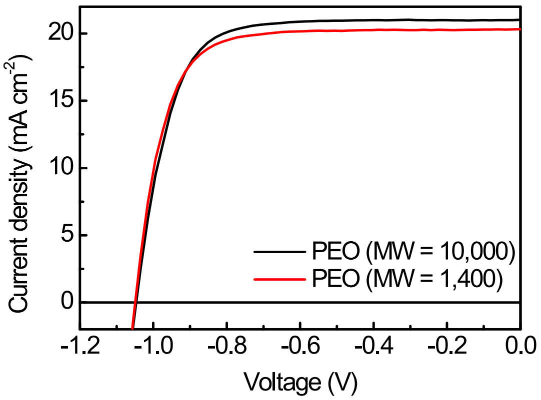

Figure S10. J-V curve of PEO-perovskite device with MW 10,000 and MW 1,400.

We also tried low MW PEO (MW = 1,400) in a perovskite device, which showed comparable performance to the PEO we used in the study (MW = 10,000). This result indicates that MW of PEO is not a determining factor for perovskite device applications.

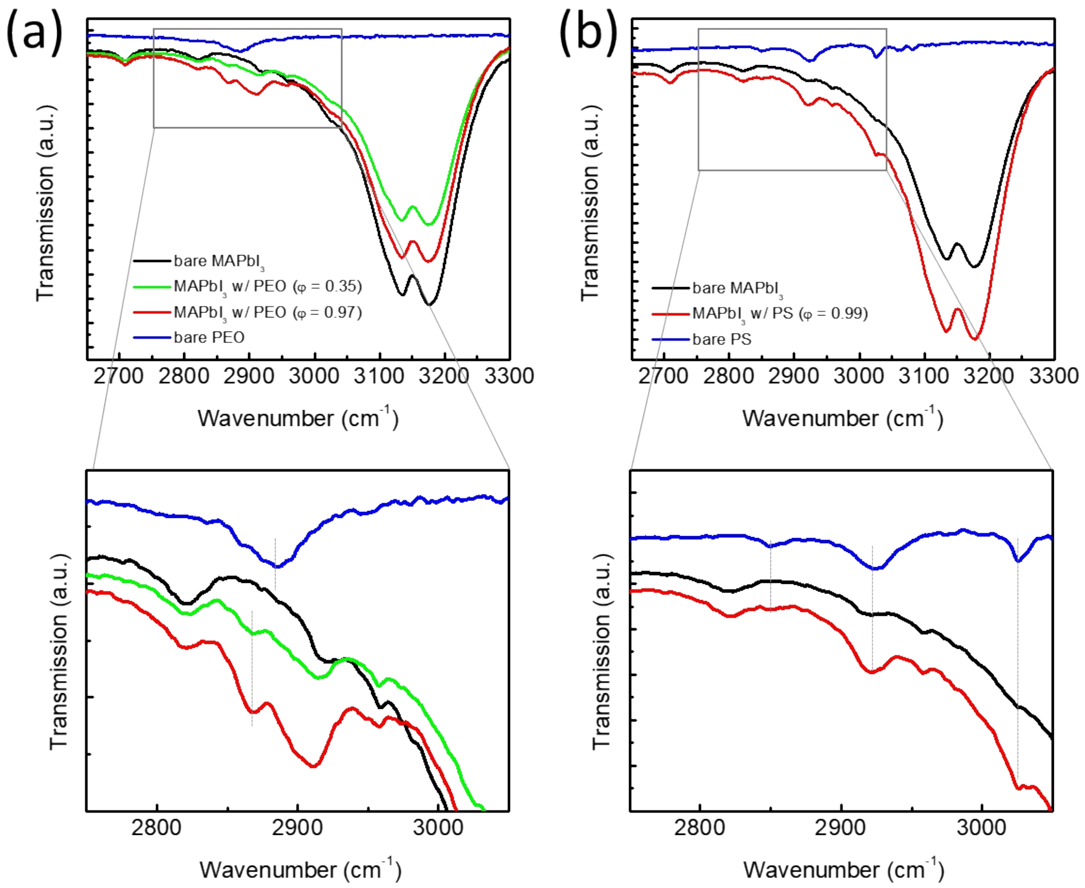

Figure S11. FT-IR spectra of MAPbI3 films with (a) PEO (1 and 10 mg·ml^{-1}) and (b) PS passivation (10 mg·ml^{-1}) and neat polymer thin films. The wavenumber range from 2700 to 3100 was magnified.

The IR spectra show peaks related to asymmetric and symmetric N–H stretching modes (3179 and 3132 cm^{-1}), asymmetric and symmetric C–H stretching modes (2958 and 2921 cm^{-1}), and various resonant modes (2817 and 2711 cm^{-1}). The positions of these peaks correspond to the reported IR spectra of pure MAPbI$_3$.[4, 5] The IR spectra of the neat PEO thin film show the characteristic peak at 2885 cm^{-1} arising from methylene stretching mode. The FTIR spectrum of MAPbI$_3$/PEO film exhibits both of the methylene stretching peak from PEO and the characteristic peaks from perovskite. Interestingly, the spectrum of MAPbI$_3$/PEO film shows that a shift of methylene stretching mode from PEO to lower wavenumber, 2868 cm^{-1} (Δ = 17 cm^{-1}), which reveals the existence of intermolecular interaction between perovskite and PEO thin layer.

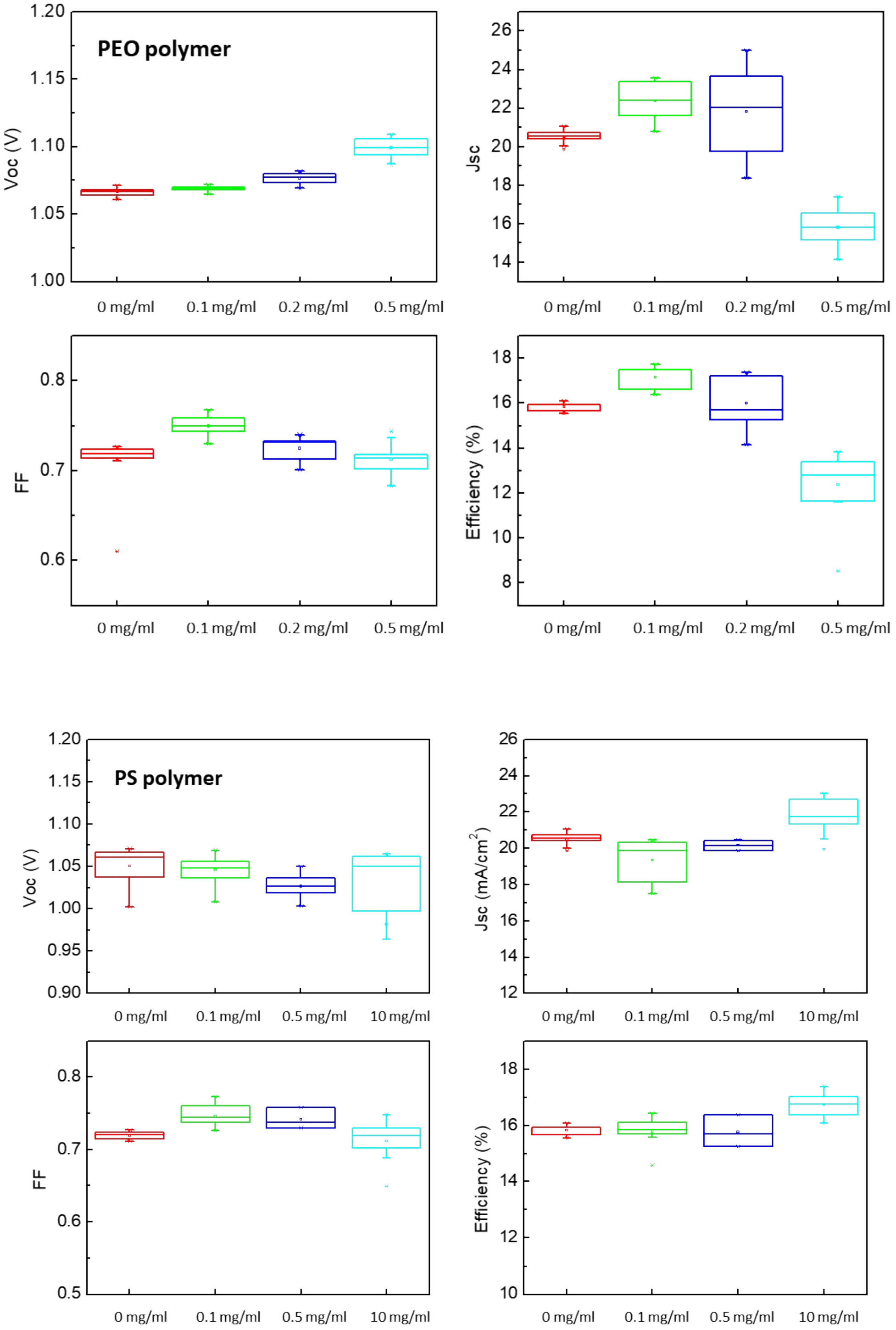

Figure S12. Device statistics of the $MAPbI_3$ devices processed with PEO and PS as a function of concentration

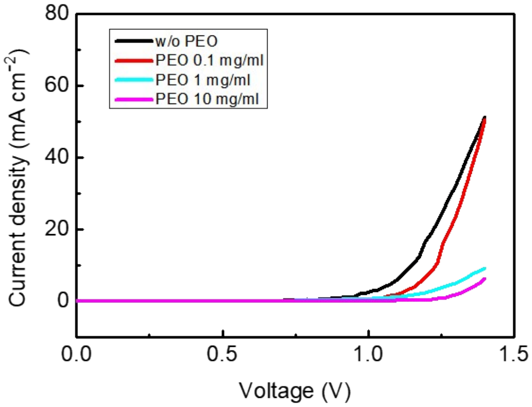

Figure S13. Dark J-V curves of the $MAPbI_3$ devices processed with PEO or PS measured in the dark.

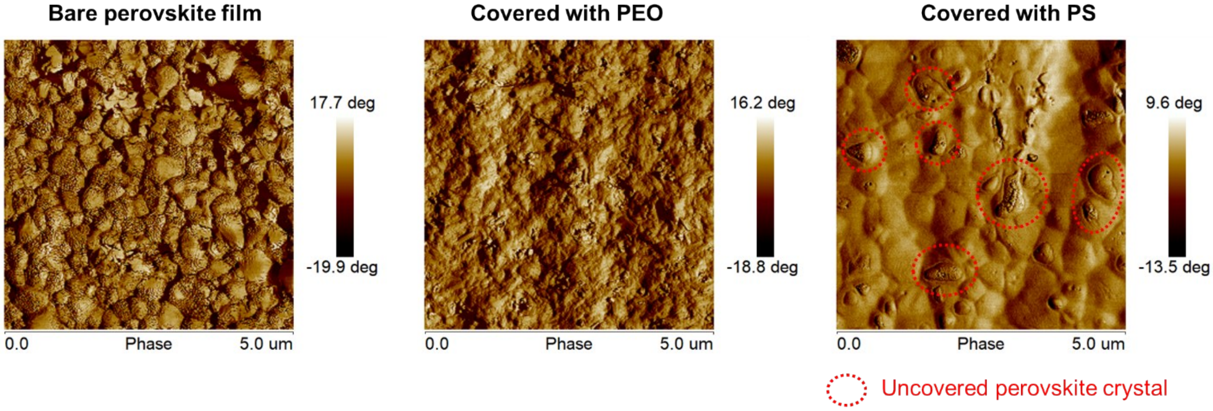

Figure S14. AFM phase images of $MAPbI_3$ coated with polymer thin films from various concentrations.

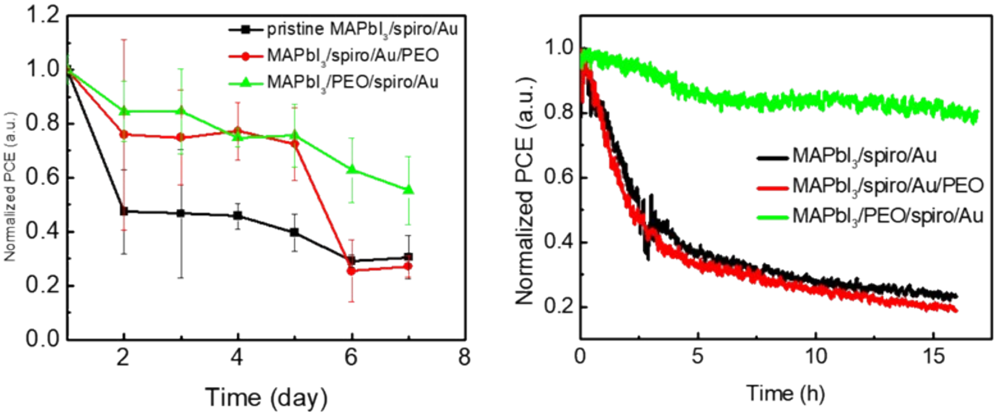

Figure S15. Time-dependent normalized PCE of perovskite films under exposure to 88% RH and MPP tracking of the device with the over-coated PEO in the ambient atmosphere.

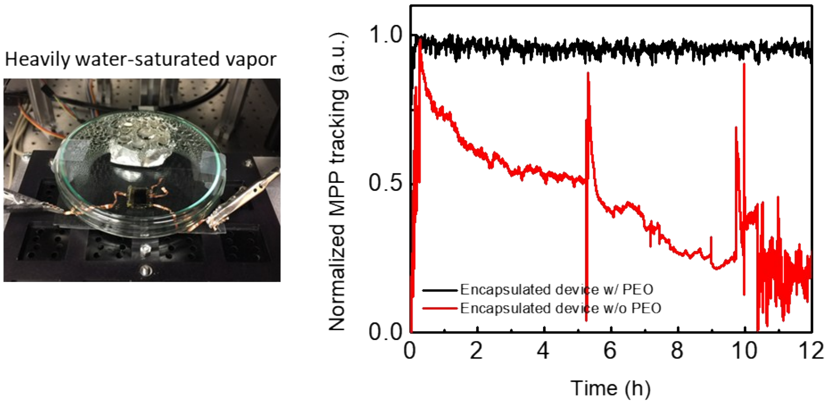

Figure S16. Maximum Point Point (MPP) Tracking of the $MAPbI_3$/PEO device with encapsulation under heavily water-saturated vapor (RH ~ 100%).

The passivation of the perovskite thin film by PEO is not meant to eliminate the solar cell encapsulation, but to relax the constraint that the encapsulating material would need (and consequently its cost). To make our point, we used commercially available epoxy adhesive (Epoxy-Kleber, 6183) and sliding glass to encapsulate devices with and without PEO interlayers, and we track their under polarization (maximum power point tracking), at1.5G AM illumination and exposed to saturated relative humidity as high as ~100%. While the device without PEO showed a continuous decrease, the device with PEO maintains 100% of its initial PCE over 13 h under 1.5 AM illumination and exposure to heavily water-saturated vapor (RH ~100%)

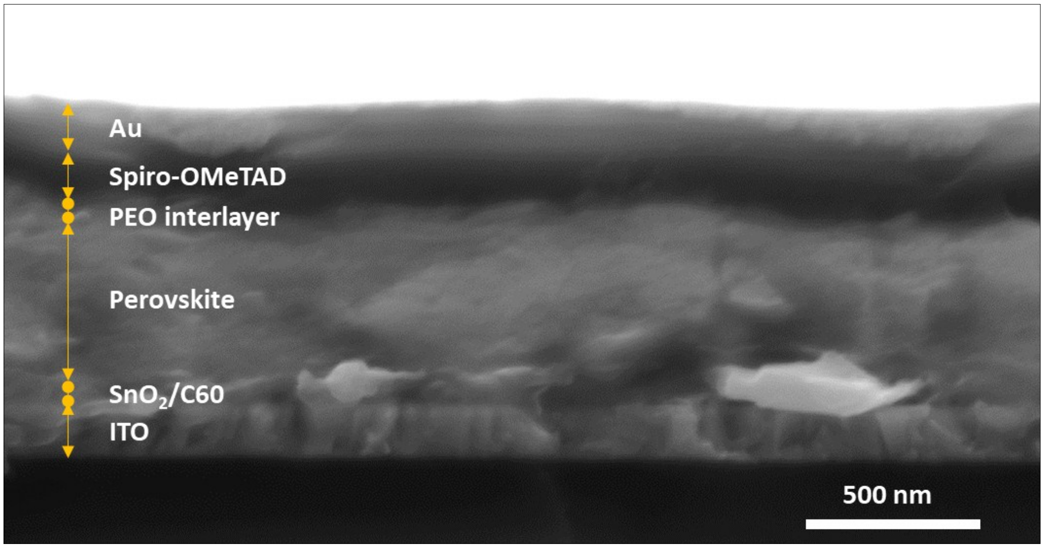

Figure S17. Cross-section SEM image of perovskite photovoltaic device with a structure of ITO/SnO_2/C_{60}/Perovskite/PEO/spiro-OMeTAD/Au.

Reference

1. S. G. Motti, M. Gandini, A. J. Barker, J. M. Ball, A. R. Srimath Kandada and A. Petrozza, *ACS Energy Lett.*, 2016, **1**, 726-730.

2. S. D. Stranks, V. M. Burlakov, T. Leijtens, J. M. Ball, A. Goriely and H. J. Snaith, *Phys. Rev. Appl.*, 2014, **2**, 034007.

3. Y. Yamada, T. Nakamura, M. Endo, A. Wakamiya and Y. Kanemitsu, *J. Am. Chem. Soc.*, 2014, **136**, 11610-11613.

4. T. Glaser, C. Müller, M. Sendner, C. Krekeler, O. E. Semonin, T. D. Hull, O. Yaffe, J. S. Owen, W. Kowalsky, A. Pucci and R. Lovrinčić, *J. Phys. Chem. Lett.*, 2015, **6**, 2913-2918.

5. Z. Zhu, V. G. Hadjiev, Y. Rong, R. Guo, B. Cao, Z. Tang, F. Qin, Y. Li, Y. Wang, F. Hao, S. Venkatesan, W. Li, S. Baldelli, A. M. Guloy, H. Fang, Y. Hu, Y. Yao, Z. Wang and J. Bao, *Chem. Mater.*, 2016, **28**, 7385-7393.